Stress Whitening Quantification of Thermoformed Mineral Filled Acrylics

E. M. Gunel[1]
e-mail: emgunel@buffalo.edu

C. Basaran
e-mail: cjb@buffalo.edu

Department of Civil, Structural and Environmental Engineering,
State University of New York at Buffalo,
Buffalo, NY 14260

Stress whitening problem in thermoformed alumina trihydrate (ATH) reinforced poly(methyl methacrylate) (PMMA) was studied. In situ heavy-gage thermoforming of acrylics was entirely replicated under laboratory controlled conditions at different operation parameters. Samples were monitored with optical microscope after the completion of the thermoforming operation. For stress whitening quantification, a new index was proposed from image histograms of processed optical micrographs. Results indicated that stress whitening in PMMA/ATH samples increases with level of plastic deformation at all thermoforming conditions. The influence of the forming rate and forming temperature on the degree of stress whitening was explained in terms of change in material behavior and microdeformation mechanisms around two characteristic temperatures of PMMA/ATH. Developed method for stress whitening quantification characterizes different levels of stress whitening with single numeric values. It is shown that stress whitening index and density of microdeformation features display a strong correlation. Higher density of particle cracks at low forming temperatures results in higher stress whitening levels. Increased surface irregularity and large size voids at high forming temperatures produce lower stress whitening. [DOI: 10.1115/1.4001262]

Keywords: thermoforming, particulate reinforced composites, image analysis, stress whitening, high temperature deformation

1 Introduction

Thermoformed acrylic particulate composites are widely used for domestic and industrial applications for which aesthetic quality of thermoformed products is a primary concern. In addition to mold design and complexity of geometry, the quality of the final product strongly depends on operation parameters such as heating period and rate, mold temperature, forming rate, and cooling rate. The failure in implementation of appropriate thermoforming conditions causes many problems in appearance and shape of thermoformed parts [1]. Solutions for these problems are mostly related to heating or forming conditions and partially the design of the mold. Appropriate changes in relevant operation parameters improve performance and quality, hence, reduced cost. Though thermoformability is closely related with material properties and sometimes limits the design of products to specific materials; extending applicability over a wider range of materials, establishing optimum parameters, and eliminating stress whitening problem is possible through understanding mechanisms and conditions causing stress whitening.

In thermoformed acrylics, stress whitening is widely observed as a result of improper thermal conditioning and/or excess drawing of insufficiently heated panels [2]. The increase in optical brightness or enhanced opacity in polymeric materials is referred as "stress whitening." Concurrently with mechanical deformation, transparent or translucent polymeric materials become opaque and attain a white appearance [3,4], while opaque materials change into a milky-white color [5–7]. Microlevel deformation studies on particulate reinforced polymers such as polypropylene [8,9], polyethylene [10,11], polybutene [12,13], and poly(methyl methacrylate) [14–19] showed that stress whitening is primarily due to the scattering of visible light from mechanically induced defects such as microvoids and microcracks. The level of stress whitening strongly depends on size and density of microvoids, and it is widely accepted that stress whitening is only observed if the size of defects is in the order of wavelength of visible light [20,21]. The relation between microscopic defect size and stress whitening was observed in polypropylene samples with different crystallinity. Dasari et al. [22] reported that large voids in high crystalline polymer absorb visible light and cause less whitening compared with low crystalline polymer, in which smaller voids scatter more visible light. Loading conditions have also a strong influence on microdeformation mechanisms and degree of stress whitening. Liu et al. [8] reported that uniaxial tensile stretching of isotactic polypropylene results in stress whitening only at low temperature and high strain rates, due to extensive fibrillation and microvoid formation.

Thermoplastic polymers generally display crazing type of plastic deformation mechanism accompanied with intense stress whitening. Recent studies on polypropylene and polyethylene indicate that stress whitened regions in tensile deformed samples include closely spaced crazes, and increased opacity was associated with light scattering from microvoids involved in the crazing mechanism [23–25]. When conditions favoring crazing are constrained such as compression loading under plane strain condition, another form of plastic deformation mechanism, shear yielding may take place in the form of distinguishable shear bands formed theoretically at about 45 deg with respect to the principle stress direction. The source of stress whitening observed in the shear yielding mechanism is considered as a strong birefringent characteristic of shear bands experiencing high plastic strains [26] or change in the refractive index of oriented rubber particles in rubber toughened polymers [27]. Nevertheless, the intensity of stress whitening in shear bands is generally less than that in crazes, and only when some other microscopic defects (cavitation or debonding of fillers) are involved in shear yielding mechanism, the intensity of stress whitening increases.

Material resistance to whitening may be improved by altering

[1]Corresponding author.

Contributed by the Materials Division of ASME for publication in the JOURNAL OF ENGINEERING MATERIALS AND TECHNOLOGY. Manuscript received April 23, 2009; final manuscript received December 10, 2009; published online June 15, 2010. Assoc. Editor: Hussein Zbib.

the crystallinity [22,24] and molecular structure of the material [28,29], or by incorporating rigid filler particles. Proper bonding of fillers to polymer matrix may improve elastic modulus and yield stress, hence, minimize severity of polymer plastic deformation. Several experimental studies indicated that clay [11–13,30], wollastonite [7,31], and calcium carbonate [5,21] reinforced polymer composites exhibit significantly reduced scratch visibility or stress whitening compared with homopolymer, which was attributed to the reinforcement effect of mineral fillers. It was also observed that the scratch hardness defined in terms of the dimension of deformation features on the scratched surface is consistent with the level of stress whitening. However, rigid particle inclusion does not always guarantee reduction in whitening. Inadequate strength and stiffness of constituents and poor interfacial bonding strength may increase stress whitening [32] and promote matrix deformation by providing effective nucleation sites for crazing or shear yielding. In such cases, the source of stress whitening is found to be cavitation (tearing) [33–37] or interfacial debonding [38,39] of rubber particles. In rigid particle filled polymers, microvoid formation may take place as a result of debonding of particles from matrix and failure of particles [7,31,40–42]. The relationship between mechanical deformation and stress whitening was also observed in the correlation between plastic deformation and stress whitening for the case of impact and fracture tests. Many researchers have shown that fracture toughness of polymer composites can be accurately estimated if the length of stress whitened region is utilized in the J-integral method [43,44] or the essential work of fracture method [45–48].

Except for radial and linear measurements of whitened regions in impact and fracture tests, a fundamental requirement for good measurement of stress whitening is that the used method should truly present the perception of the human eye [13]. Though it is empirical and not reliable, qualitative measurements based on naked-eye observations were formerly used to explain the variation in stress whitening with different test conditions [8], composition of polymers [38,39]. Based on the change in reflectivity of opaque materials and change in refractive index of transparent materials, several measurement methods for stress whitening quantification were developed such as light transmittance intensity [49–52], reflected polarized light intensity [41], and direct color measurements from spectrophotometer [53,54]. Misra and coworkers [11,12] developed a new method that quantifies stress whitening in terms of change in gray scale, obtained from optical images of deformed regions. This method is only limited to qualitative comparison of the gray level change (ΔG) profiles of different composites and loading conditions [20,21]. However, a numeric value representing the level of stress whitening of an admissible region will be more valuable in developing a relation between stress whitening and mechanical deformation parameters, as well as understanding the influence of loading conditions and other material properties on stress whitening. In the present work, a new stress whitening quantification method is proposed, based on image histograms of optical micrographs. According to the developed method, stress whitening can be characterized with a single numerical value. The influence of thermoforming conditions on stress whitening in thermoformed acrylic particulate composites has been studied in terms of stress whitening indexes obtained through this new method.

2 Experimental Procedure

2.1 Materials. The material used in this study is poly(methyl methacrylate) (PMMA) filled with alumina trihydrate (ATH) particles [55]. PMMA has a glass transition temperature (T_g) around 100°C and a number-average molecular weight (M_n) of 150 kg/mol. The average particle size of ATH agglomerates is 30–40 μm, and the particle volume fraction in acrylic composite is 50%. ATH inclusion in PMMA specifically improves dimensional stability and flame resistance of the polymer matrix. ATH agglomerates are irregular in shape and they are strongly bonded to PMMA matrix by means of adhesion promoting agent [56]. In addition, thermal microstress fields around agglomerates due to the coefficient of thermal expansion (CTE) mismatch between filler/matrix disappears at temperatures above 90°C [57]. Since the stress level around fillers may reach 15–75% of tensile yield strength of composite upon cooling, thermal microstress due to CTE mismatch plays an important role in the failure of particulate composites under thermomechanical loading conditions.

2.2 Thermoforming Experiments. In thermoforming tests of PMMA/ATH, uniaxial tension tests were preferred due to experimental simplicity in application and interpretation [58–61]. Standard ASTM D638 Type IV specimens [62] were cut from commercially available extruded acrylic particulate composite (PMMA/ATH) panels. Similar to the conventional heavy-gage thermoforming procedure, samples were first heated at 150°C for 20 min in VWR Signature™ Horizontal Airflow type convection oven. Heated specimens were stretched to different levels of deformation in a servomechanical MTS material testing unit type 858 table top system (1 kN to 10 kN capacity) controlled by a computer and fitted with an ATS 7510 box thermal chamber for the control of ambient temperature. In order to prevent extrusion of material from grips, minimum possible grip pressure was employed. Grip slip was not observed due to special serration pattern on grip wedges. Initial distance between grips was kept at a minimum possible level, such that uniaxial stretching was confined to the neck-down portion of the dogbone sample [1].

The test procedure includes three steps: first, the loading step corresponding to forming step; second, the dwell step corresponding to cooling step, and third, the unloading step corresponding to removal of sample from mold. The forming rate was chosen at three different displacement rates as 0.9 mm/s, 0.09 mm/s, and 0.009 mm/s. Forming temperatures representing different mold temperatures were selected as 30°C, 50°C, 75°C, 90°C, 100°C, 125°C, and 140°C. During the forming step, the temperature was held fixed in the thermal chamber representing the desired mold temperature. At the beginning of the dwell step, the thermal chamber door was opened for cooling of the sample, and deformation in the specimen was held fixed. Unloading at a high rate was preferred in order to characterize the rapid removal of the thermoformed part from the mold. Successive thermoforming applications on the same sample were planned to determine stress whitening at different levels of deformation. Samples were tested for five times with increasing deformation in each subsequent thermoforming cycle. The deformation limits in the forming step were established as 4.5 mm, 6.75 mm, 9 mm, 13.5 mm, and 18 mm. The results presented herein are the arithmetic average of the results obtained from five separate tests conducted at the same condition.

2.3 Stress Whitening Evaluation. Stress whitening in thermoformed samples was determined on the basis of the change in optical appearance between undeformed and deformed state. Specimens were monitored by Panasonic GPKR222 CCD camera with adjustable illumination. The screening area on the surface of the sample is 2 mm by 2.5 mm in the middle of the specimen, away from any stress concentration zones. Midsections of the specimens were marked with a marker so that the same location would be monitored at all cases. Great care was taken to maintain the same brightness level in all optical images. Optical micrographs were recorded before any test (virgin state) and at the end of each thermoforming cycle (thermoformed state). Recorded images were first converted to gray mode from red-green-blue color mode using Adobe® Photoshop® software. Processed images were then digitized using MATLAB® Image Processing Toolbox™ software and image histograms were obtained in gray scale. An index describing the overall optical appearance of the monitored region was derived from image histograms. Finally, stress whitening in thermoformed samples was numerically quantified as the differ-

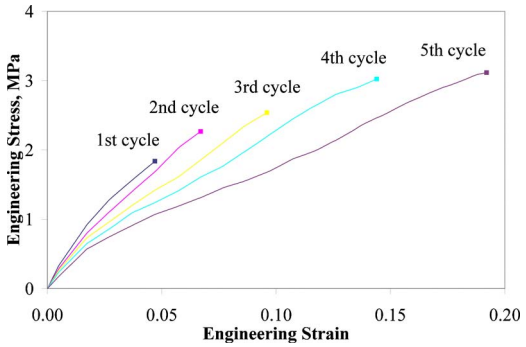

Fig. 1 Engineering stress-strain curves of PMMA/ATH samples in forming step at 0.9 mm/s forming rate, 75°C forming temperature

ence between indexes corresponding to the virgin and thermoformed states.

2.4 Scanning Electron Microscopy (SEM). Microdeformation features on the surface of thermoformed PMMA/ATH samples were studied using scanning electron microscopy (SEM, HITACHI S4000) in the secondary electron imaging mode. All samples were cryofractured at the ends without damaging the thin midportion and carbon coated prior to examination. Scanning electron micrographs were also used for the quantification of surface deformation features on thermoformed PMMA-ATH samples. Damaged zones observed in SEM images were layered and isolated from undamaged parts using Adobe® Photoshop® software. Next, areal densities of damaged zones were calculated using particle analysis option in IMAGEJ software.

3 Results and Discussion

3.1 Mechanical Properties. Engineering stress-strain curves for the forming step at 0.9 mm/s forming rate and 125°C forming temperatures is presented in Fig. 1. PMMA/ATH samples were heated to 150°C prior to testing. During the forming step, specimen temperatures at 0.9 mm/s and 0.09 mm/s forming rate tests were not constant. At 0.009 mm/s forming rate, the specimen temperature was nearly constant through testing. While specimens were stretched, they were also cooling down to environmental chamber temperature (or mold temperature). This situation is identical to industrial heavy-gage thermoforming procedure during which panels start cooling immediately at the forming stage. The cooling rate during the forming step depends on the difference between the specimen temperature and forming temperature. Cooling is much faster at low forming temperatures. If the forming rate is higher than the cooling rate (e.g., 0.9 mm/s forming rate), the specimen temperature is always larger than the forming temperature. If forming is slower than cooling (e.g., 0.009 mm/s forming rate), specimens completely cool down to forming temperature. Since cooling at forming temperatures above 100°C is insignificant, samples were stretched at nearly constant temperature, regardless of the forming rate [63].

Repeated thermoforming cycles on the same sample cause strength and stiffness degradation because of damage evolution in the material (Fig. 1). Irreversible damage induced by successive thermoforming cycles varies with forming temperature and rate. Damage evolution limits the possible number of the thermoforming operation on PMMA/ATH specimens, especially at low temperatures. The number of thermoforming cycles before failure of PMMA/ATH samples at different conditions is presented in Table 1. As a result of heat application at the beginning of each thermoforming cycle, plastic deformation in the polymer matrix alone was recovered similar to polymer healing upon heat treatment, while damage in ATH agglomerates and in interphase between filler and matrix was not recovered. Strength degradation in stress-strain curves clearly indicates that complete healing did not occur, though specimens were heated to 150°C between thermoforming cycles. By means of this healing process prior to testing, the part of damage associated with polymer matrix was reversed to some extent, and composite strength and stiffness at early stages of deformation (for strain values less than 2%) did not change significantly with the increasing number of thermoforming cycles. Material degradation was only pronounced at high strain levels where the increasing damage in mineral fillers cause noticeable change in stiffness and strength.

Table 1 Number of possible thermoforming cycles before failure of PMMA/ATH samples at different conditions (na: not applicable)

		Forming temperature (°C)						
No. of cycles		30	50	75	90	100	125	140
Forming rate (mm/s)	0.9	3	4	4	5	5	5	5
	0.09	na	1	3	4	5	5	5
	0.009	na	na	1	3	5	5	5

The typical loading-displacement history of thermoforming tests are presented in Fig. 2. Following the forming step, the environmental chamber door was opened and specimens were left for cooling at room temperature while deformation at the end of forming step was kept constant during cooling period. In the cooling step, behavior of PMMA/ATH samples is governed by two counter-acting phenomena. At the beginning of the dwell step, the stress values drop by some amount because of stress relaxation of polymer matrix, whereas continuous cooling increases tensile stress in the sample induced by thermal shrinkage at constant deformation level. The competition between stress relaxation and thermal stress determines the maximum experienced tensile stress throughout the thermoforming procedure. The effect of stress relaxation is more pronounced at high forming rates, while the effect of thermal stress is more pronounced at high forming temperatures. In the unloading step, elastic recovery takes place to different extent, depending on the forming rate and temperature, yet recovered elastic strain is less than 0.1% of the total strain at all thermoforming conditions.

3.2 Surface Microdeformation in Thermoformed Mineral Filled Acrylics. Thermoforming conditions strongly influence microdeformation mechanisms and overall response of PMMA-ATH [63]. Depending on the forming rate, forming temperature, and deformation limit, different forms of mechanisms were observed in thermoformed PMMA/ATH samples. The SEM image of the

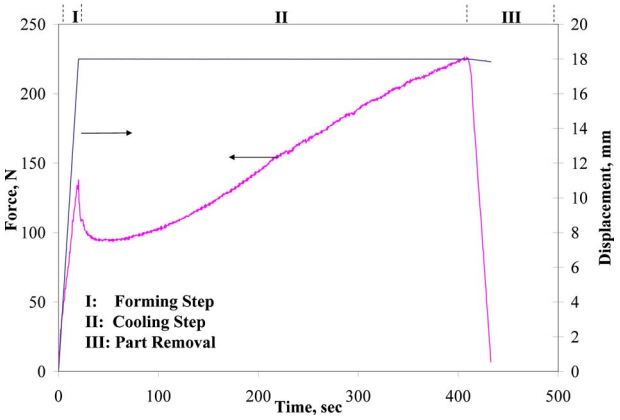

Fig. 2 Loading-displacement history of PMMA/ATH sample thermoformed at 0.9 mm/s forming rate, 75°C forming temperature (deformation limit 13.5 mm)

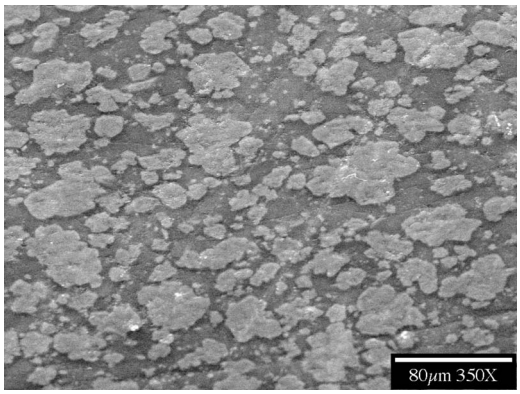

Fig. 3 SEM images of undeformed PMMA/ATH sample

undeformed PMMA/ATH sample is presented in Fig. 3. Particle size distribution of ATH fillers is quite large and ATH agglomerates are randomly dispersed in the PMMA matrix. Surface deformation features associated with stress whitening was studied on samples from last available thermoforming cycles. SEM images of PMMA/ATH samples thermoformed at different forming temperatures and rates are presented in Figs. 4–6. The intensity and type of surface deformation features of thermoformed PMMA/ATH samples change significantly around 100°C (T_g of matrix) and 90°C, at which the influence of the thermal stress due to CTE mismatch diminishes. SEM images show that the main failure

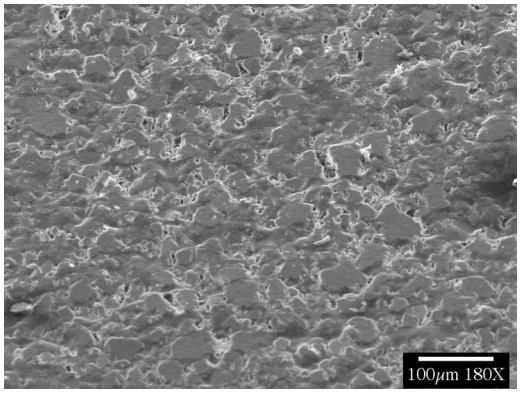

Fig. 4 SEM images of thermoformed PMMA/ATH samples at 0.9 mm/s forming rate and 90°C forming temperature (fifth thermoforming cycle)

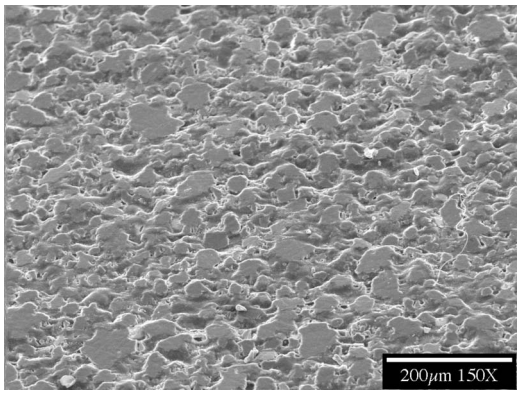

Fig. 5 SEM images of thermoformed PMMA/ATH samples at 0.09 mm/sec forming rate and 125°C forming temperature (fifth thermoforming cycle)

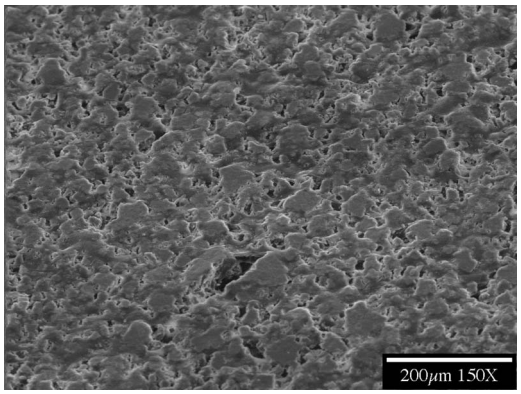

Fig. 6 SEM images of thermoformed PMMA/ATH samples at 0.009 mm/s forming rate and 100°C forming temperature (fifth thermoforming cycle)

mechanism at temperatures below T_g of PMMA is particle cracking (Figs. 4 and 6). At temperatures above 100°C, combined interfacial failure and particle disintegration with ductile tearing of matrix were observed (Fig. 5). However, the main source of stress whitening in all cases is the light scattering entities formed by failure of ATH agglomerates. The influence of thermal stress due to CTE mismatch diminishes as the temperature increases and the thermal microstress around ATH particles reduces. As a result, particle failure decreases as forming temperature increases up to T_g of the matrix (Fig. 4). At temperatures around T_g of the matrix, polymer matrix becomes more flexible, while ATH remains rigid, regardless of the forming temperature since ATH has a melting temperature around 3500°C. Due to increased polymer chain mobility, the intensity of particle cracking also increases around 100°C forming temperature (Fig. 6). At higher forming temperatures ($T > 100$°C), the source of microdeformation mechanism is completely different than colder forming temperatures. At these forming temperatures, the matrix is more like in a semiliquid form. ATH fillers are prone to cracking at a higher level, because surrounding highly mobilized polymers have a tendency of flowing rather than deforming coherently with agglomerates (Fig. 5). Severe stretching of highly mobilized polymer chains leads to failure in particle-matrix interphase, observed as isolated large size particles and disintegration of ATH agglomerates because of completely incompatible deformation capabilities of the two constituents (Fig. 5). The increase in surface irregularity at high forming temperatures (100°C, 125°C, and 140°C) hinders stress whitening to some extent because light is scattered into many directions from irregular surfaces [31,32]. Similarly, large size voids or cavities (at 100°C and 125°C forming temperature) also absorb light instead of scattering, which results in the lower stress whitening level [13,21].

3.3 Optical Micrographs. The stress whitening quantification based on gray scale became a popular method in the last decade [7]. Change in appearance is expressed as difference in grayness levels of sample at undeformed and deformed state. For an 8 bit-grayscale image, different shades of gray are defined for each pixel as a brightness value between 0 (black) and 255 (white). In this study, midsections of specimens were monitored at the end of each thermoforming cycle for quantitative local evaluation of stress whitening. Examples of processed optical images of the thermoformed PMMA/ATH sample are presented in Fig. 7. The increase in stress whitening with the increasing number of thermoforming cycles can be observed as a change from darker to brighter appearance in images. In the optical image of virgin sample (Fig. 7(*a*)), there are two distinguishable phases: matrix and filler appearing as black regions and gray regions, respectively. In the first three cycles (Figs. 7(*b*)–7(*d*)), short-length,

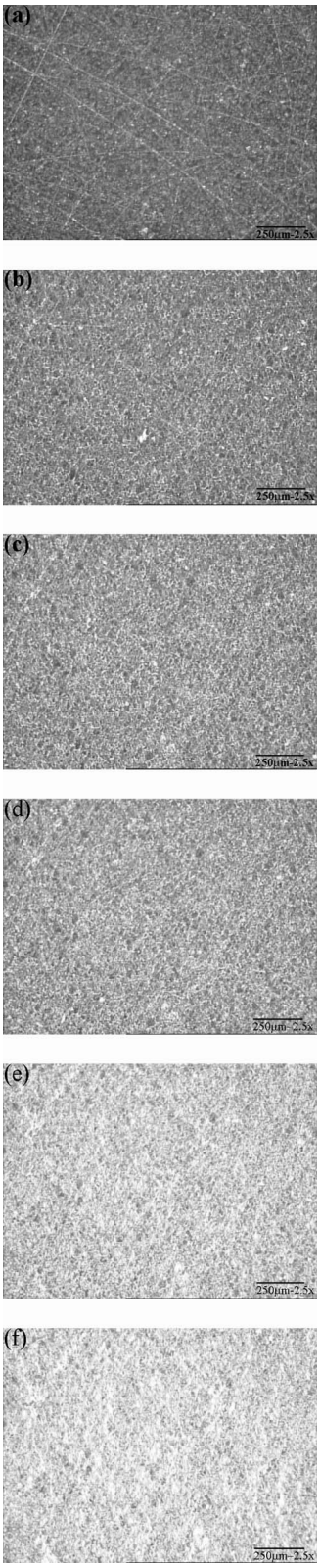

Fig. 7 Processed optical images of thermoformed PMMA/ATH sample at 0.009 mm/s forming rate, 100°C forming temperature (*a*) at undeformed state and at the end of (*b*) first, (*c*) second, (*d*) third, (*e*) fourth, and (*f*) fifth thermoforming cycle

bright strips of light scattering entities start to appear and density of these strips increases with increasing number of thermoforming cycles. In the last two cycles (Figs. 7(*e*) and 7(*f*)), the density and size of these scattering entities become so large that they dominate general appearance of picture. It is clear from optical images in Fig. 7 that stress whitening in thermoformed PMMA/ATH samples is primarily due to appearance of these bright strips on the surface. Microstructural studies showed that light scattering entities on the surface of thermoformed samples were actually failure zones within and around ATH agglomerates. At low forming temperatures ($T<100°C$), many densely packed cracks were present in ATH agglomerates, while combined particle disintegration and interfacial failure were dominant failure mechanisms at high forming temperatures ($T>100°C$). Different levels of stress whitening were observed in thermoformed PMMA/ATH samples, depending on the mode of deformation and density of light scattering features.

3.3.1 Stress Whitening Index. After digitizing recorded optical images, histograms at undeformed and deformed state of samples were plotted in gray scale. Image histograms of optical images of two different thermoformed PMMA/ATH samples are presented in Fig. 8. Stress whitening intensification in optical images (Figs. 7(*a*)–7(*f*)) is observed as a shift to higher gray values in histograms (Fig. 8(*a*)). Since total number of data points (pixels) is constant, and the same location is monitored in all optical images, increase in level of stress whitening means that pixels with small gray values in previous cycles have larger gray values in the following cycles. The influence of thermoforming conditions on stress whitening is also emphasized in gray level distribution trends at different cycles. At 0.009 mm/s forming rate and 100°C forming temperature (Fig. 8(*a*)), stress whitening in the first three cycles is pronounced as a remarkable right-shift from the undeformed state histogram. In the last two thermoforming cycles (Fig. 8(*a*)), accumulation of data points in a narrow band of high gray levels (150–255) is a clear indication of higher levels of stress whitening. Lower stress whitening in thermoforming of PMMA/ATH samples at 0.9 mm/s forming rate and 75°C forming temperature (Fig. 8(*b*)) is observed as a minor shift in gray level and very closely spaced distribution curves of different cycles.

For quantitative comparison of stress whitening at different thermoforming conditions, it is essential to derive a descriptive estimator from image histograms in Fig. 8. A plausible approach is to assume that histograms are normally distributed in the range of 0–255, and to define an estimator, based on the location parameter of normal distribution. In practice, the Gaussian model is a suitable model to fit histogram distributions in optical images, similar to magnetic resonance images [64]. Gray level in a pixel is the weighted sum of a large number of random variables associated with imaging technique. Thus, according to the generalized central limit theorem, each pixel in the image has an asymptotic Gaussian distribution. Due to limits on gray scale (0–255), this distribution is truncated [65,66]. Since optical image is composed of numerous pixel points, corresponding image histogram has also a truncated normal distribution. From a statistical point of view, this assumption can be tested by using normality tests [67]. In these tests, the hypothesis that image histograms are normally distributed was rejected because of the difference between theoretical and empirical normal cumulative distribution functions obtained from sample statistics. It should be also noted that normality tests for large sample sizes can be misleading (in this case, $>10^5$ data points or pixels), because they generally detect statistically significant but practically unimportant deviations from normality. Therefore, graphical techniques were preferred in assessment of normality of distributions instead of normality tests.

In order to investigate any possible source of non-normality in image histograms, normal probability plots were used. Normal probability plots of image histograms in Fig. 8(*a*) are presented in Fig. 9. If distributions have normal distribution, data values will follow a hypothetical straight line (dashed straight lines in Fig. 9). Deviations from linearity in normal probability plots in Fig. 9 indicate skewness of distributions. Large amount of data points below 0.1% probability show heavy-tailedness of the data set and

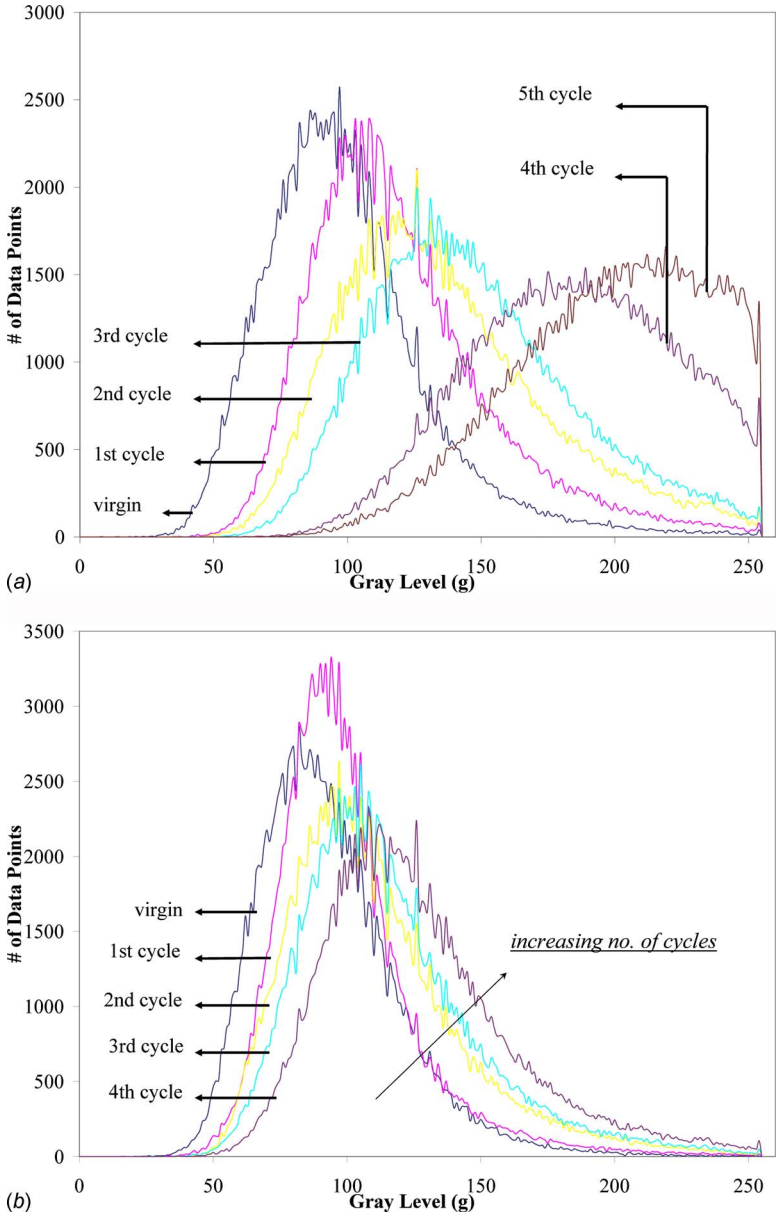

Fig. 8 Image histograms of thermoformed PMMA/ATH sample (*a*) at 0.009 mm/s forming rate, 100°C forming temperature and (*b*) at 0.9 mm/s forming rate, 75°C forming temperature

possible outliers. Skewness in data distributions can be also observed in Fig. 8(*a*), such that image histograms of undeformed sample and first three cycles have long tails above the mean (positive-skew). On the other hand, accumulation of data points and nonlinearity at gray values larger than 250 is an indication of truncated normal distribution. Based on these observations, it was concluded that causes of rejection in normality tests were outliers and skewness in distributions. For improvement of normality of data sets, skewness can be handled with proper data reflection and transformation methods, while outliers can be disregarded [68]. Before data transformation, image histograms do not conform to typical symmetrical normal distribution structure because of skewness in distribution, and estimators derived from these distributions becomes inconvenient for comparison of stress whitening at different thermoforming cycles. It is also necessary to use a unique data transformation that can reflect slight changes in stress whitening, as depicted in Fig. 8(*b*). In order to eliminate positive skewness in distributions, image histograms were plotted in natural logarithm of gray scale. Image histograms after data transformation are presented in Fig. 10.

Image histograms plotted in natural logarithm of gray scale (Fig. 10) display remarkable improvement in structure of distribution, compared with ones in Fig. 8. Data points are scattered symmetrically around the mean value. Image histograms still preserve the original stress whitening evolution trend with increasing thermoforming cycles. There is also a significant change in the linearity of data set in normal probability plot, as presented in Fig. 11. After logarithmic data transformation, there are still outliers in data sets; yet, the major part of data points follow linear lines, which is required for normality of data distribution. As a result, the central tendency of image histograms in logarithmic scale can be used for stress whitening quantification. Image histograms in Fig. 10 were characterized with two parameters, mean and vari-

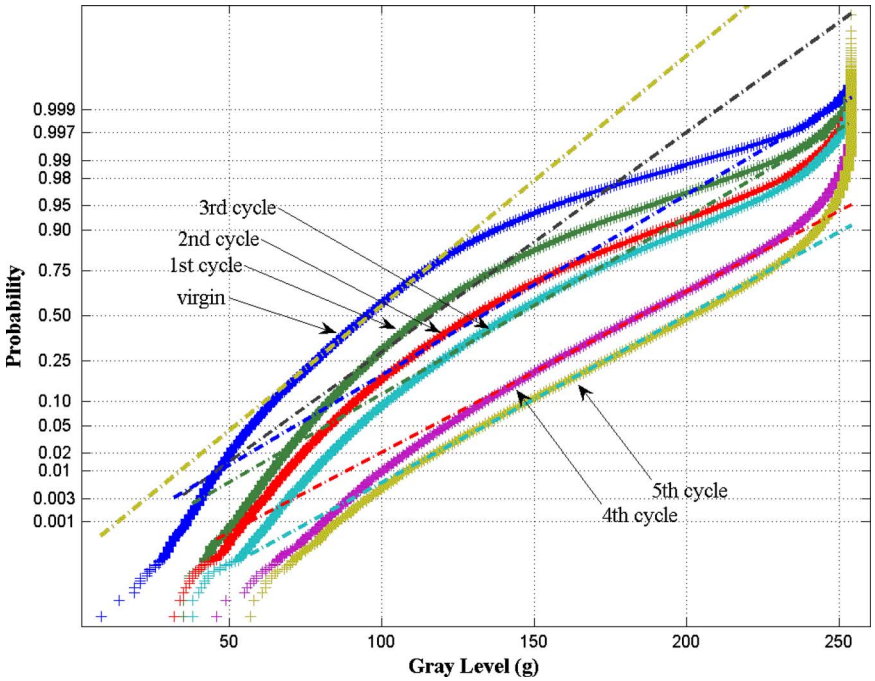

Fig. 9 Normal probability plots of image histograms of thermoformed PMMA/ATH sample at 0.009 mm/s forming rate, 100°C forming temperature

ance, as defined in Eqs. (1) and (2), where n_i is the number of data points corresponding to g_ith gray level between 0–255, and N is the total number of data points

$$\text{mean:} \quad \hat{\mu} = \frac{\sum n_i \ln(g_i)}{\frac{n_i}{N}} \tag{1}$$

$$\text{variance:} \quad \hat{\sigma}^2 = \frac{\sum n_i (\hat{\mu} - \ln(g_i))^2}{\frac{n_i}{N}} \tag{2}$$

According to proposed method, stress whitening in thermoformed PMMA/ATH samples is quantified based on optical images of a 2 mm by 2.5 mm region at the midsection. The monitored region is big enough, such that estimators derived from image histograms can be used for assessment of stress whitening observed in this region. It is also small in size, such that the variation in color intensity from adjacent parts is insignificant. As previously mentioned, central tendency of image histograms might be a good estimator, but in the presence of outliers located at lower gray levels, mean values of image histograms underestimate the level of stress whitening. Instead of the mean value, a new estimator defined in Eq. (3) is proposed as the stress whitening index of thermoformed samples. This estimator uses only pixel points with gray values larger than some threshold value defined in Eq. (4), where $\hat{\mu}_{\text{vir}}$ and $\hat{\sigma}_{\text{vir}}$ are the mean and standard deviation of the virgin sample's image histogram, respectively. By means of this filtering, the effect of outliers on the stress whitening index is minimized while all dominant data points with high gray values are included in the calculation of the index. Finally, the stress whitening level is defined as the difference between the index of the kth thermoforming cycle and index of virgin state, as shown in Eq. (5)

$$G = \frac{\sum_{g_i \geq (\hat{\mu} - \hat{\sigma})_{\text{virgin}}} n_i \ln(g_i)}{N} \tag{3}$$

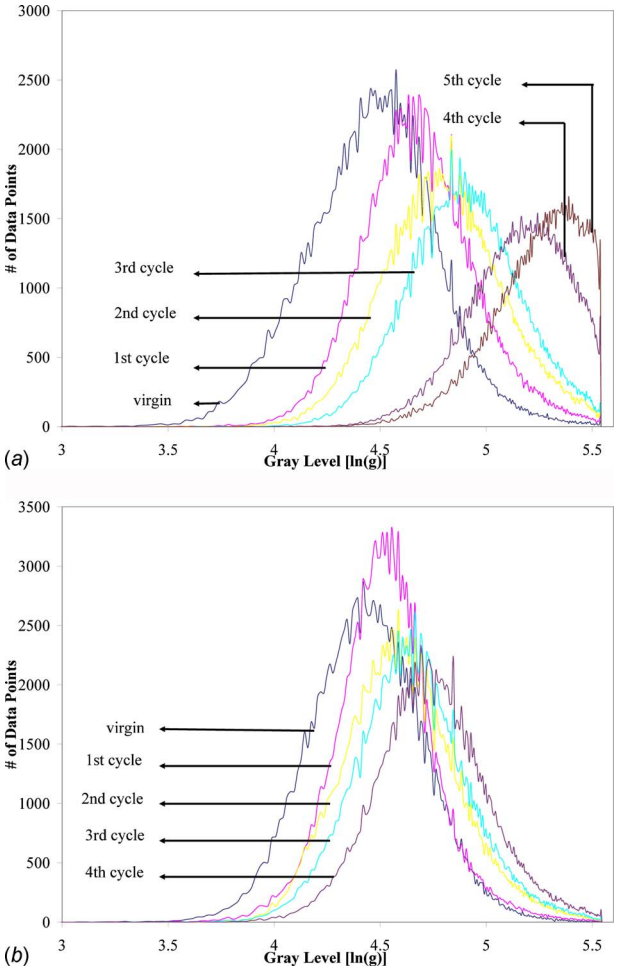

Fig. 10 Image histograms of thermoformed PMMA/ATH sample (*a*) at 0.009 mm/sec forming rate, 100°C forming temperature and (*b*) at 0.9 mm/s forming rate, 75°C forming temperature (gray level in natural logarithmic scale)

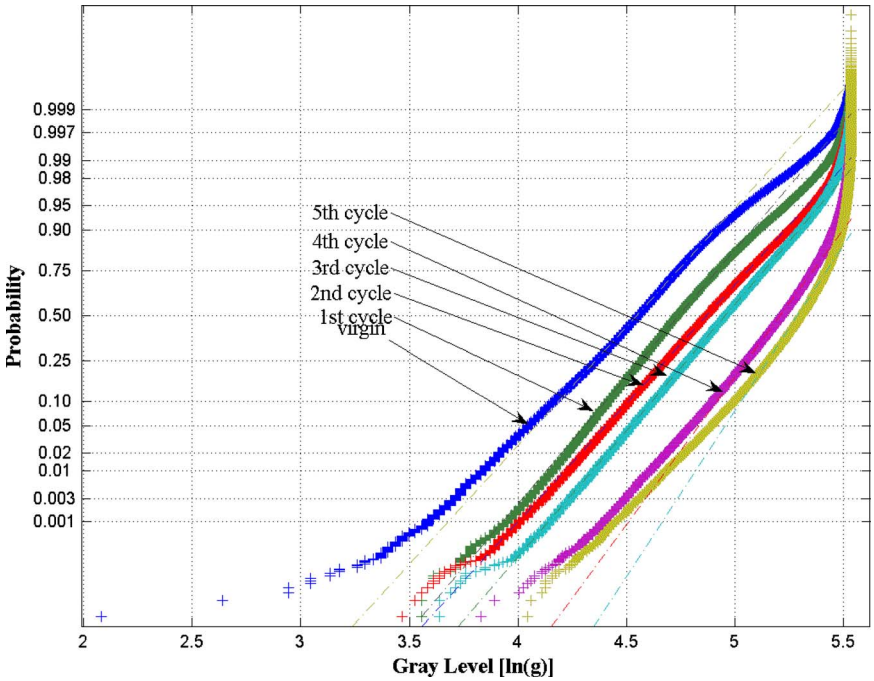

Fig. 11 Normal probability plots of image histograms of thermoformed PMMA/ATH sample at 0.009 mm/s forming rate, 100°C forming temperature (gray level in natural logarithmic scale)

$$g_i \geq (\hat{\mu} - \hat{\sigma})_{\text{virgin}} \tag{4}$$

$$\Delta G = G^{k\text{th cycle}} - G^{\text{virgin}} \tag{5}$$

3.3.2 Stress Whitening Evolution in Thermoforming Cycles. After establishing the index for stress whitening (Eqs. (3) and (5)), it is now possible to quantify stress whitening observed under various thermoforming conditions. Stress whitening levels in thermoformed PMMA/ATH samples at different forming temperatures and rates are presented in Fig. 12. For all forming conditions, stress whitening intensity increases as the number of thermoforming cycle increases. Higher deformation levels in successive thermoforming cycles induce formation and enlargement of more defects on the surface of sample, which cause higher stress whitening level to some extent. Therefore, stress whitening is actually accumulating in successive thermoforming cycles, and level of stress whitening at individual thermoforming cycles depends on previous thermoforming history of the sample. The influence of thermoforming conditions on stress whitening is pronounced through the dependence of the specimen temperature on the forming rate and temperature, as described in Sec. 3.1. At the same time, the polymer matrix deformation behavior and state of stress around ATH fillers control the microdeformation mechanism on the surface of PMMA/ATH samples and result in the variation in stress whitening with respect to the forming rate and temperature for the same level of deformation.

At 0.9 mm/s forming rate (Fig. 12(*a*)), specimen temperature was higher than the forming temperature. As a result, the temperature sensitivity of stress whitening at 0.9 mm/s forming rate is more complicated than those at 0.09 mm/s and 0.009 mm/s forming rates. Stress whitening values continuously decrease from 30°C to 75°C forming temperature, which was attributed to decrease in influence of the thermal microstress field around ATH fillers with increasing temperature. The increase in stress whitening at 90°C forming temperature compared with 75°C, indicates change in behavior of polymer matrix, resulting in incompatible deformation between constituents. Since at 0.9 mm/s forming rate, the specimen temperature is higher than the forming temperature, transition in polymer matrix characteristics was observed at 90°C forming temperature. Lower stress whitening values at 100°C was attributed to further reduction in stiffness of PMMA compared with lower temperatures. Higher stress whitening at 125°C forming temperature is related to severe plastic deformation in polymer matrix. At 140°C forming temperature, change in mode of microdeformation mechanism from particle cracking to particle disintegration causes lower stress whitening.

At 0.09 mm/s forming rate (Fig. 12(*b*)), specimens have temperatures close to the forming temperature at the end of the forming step, and the variation in stress whitening values with forming temperature can be simply classified into two regimes. At forming temperatures below 90°C, stress whitening values increase as temperature decreases because of the pronounced effect of the thermal microstress field around ATH particles. At temperatures above 100°C, the decrease in stress whitening with increasing forming temperature is related to the reduction in stiffness of the polymer matrix. Higher stress whitening level at 100°C, compared with 90°C, is attributed to the change in deformation behavior in the polymer matrix, inducing larger stress values around ATH particles. At high forming temperatures (125°C and 140°C), mode of deformation on the surface of thermoformed samples change from particle cracking to particle disintegration and interfacial failure. At the same time, severe polymer matrix deformation took place in the form of ductile drawing and tearing. These surface features at 125°C and 140°C forming temperatures results in lower stress whitening compared with forming at 100°C.

At 0.009 mm/s forming rate (Fig. 12(*c*)), complete thermal equilibrium of the specimen was achieved before completion of the forming step, and the slow forming rate allows reorganization of polymer chains. For all thermoforming cycles at 0.009 mm/s forming rate, stress whitening decreases as forming temperature increases. Relatively larger decrease in stress whitening between 75°C and 90°C is related to the significant drop in thermal microstress due to CTE mismatch, while moderate decrease at higher temperatures is attributed to slight reduction in stiffness of polymer matrix. At 0.009 mm/s forming rate, the transition in polymer

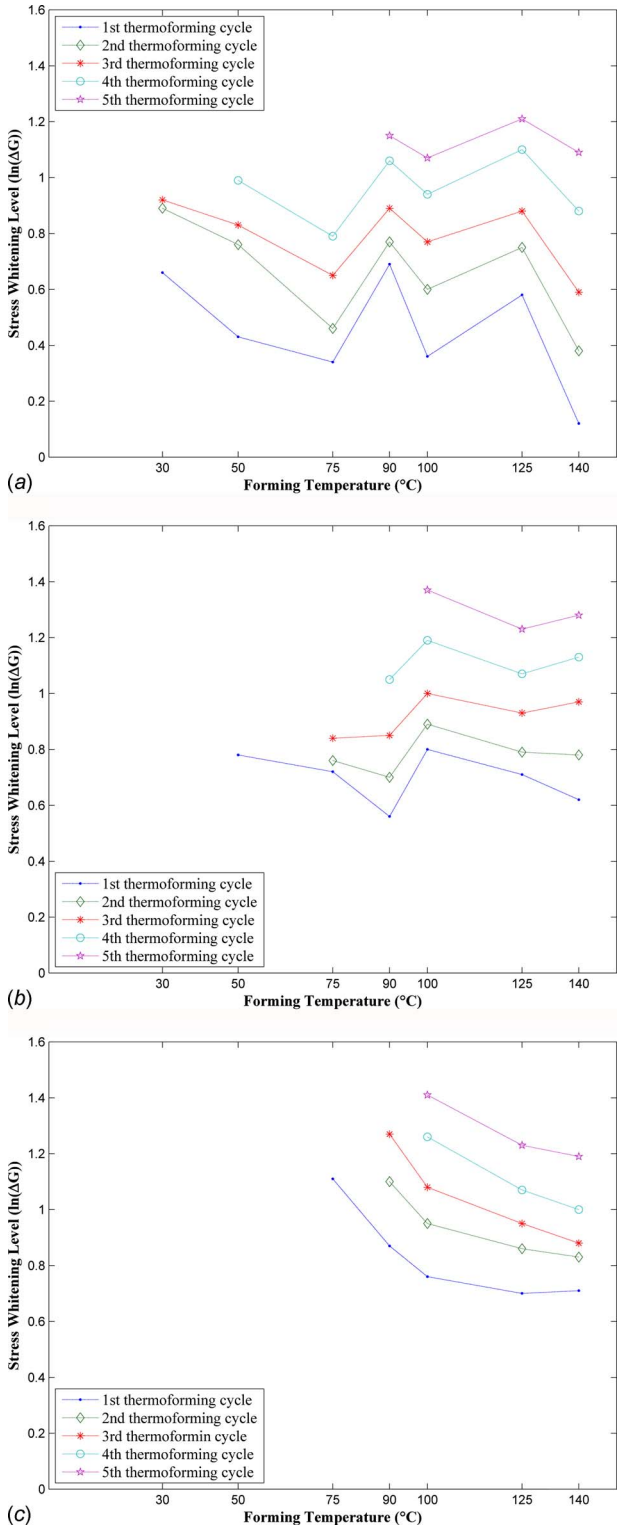

Fig. 12 Change in stress whitening ΔG in thermoformed PMMA/ATH sample at (*a*) 0.9 mm/s, (*b*) 0.09 mm/s, and (*c*) 0.009 mm/s forming rate

matrix behavior causes lower stress whitening compared with forming at 90°C. Further decrease in stress whitening at 125°C and 140°C forming temperatures is related to change in deformation mechanism at high forming temperatures.

In order to asses the relationship between stress whitening index (ΔG) and intensity of surface deformation features, SEM images of surface of PMMA/ATH samples from the last thermoforming cycles were analyzed. Scanning electron microscopy imaging requires trimming specimen into a smaller size. Since samples cannot be used anymore after such alteration in structure and it was planned to observe damage accumulation under successive thermoforming application on same samples, only samples from the last thermoforming cycles were monitored. Damaged zones in SEM images consist of mostly cracks within ATH agglomerates and partially voids formed by interphase failure. Areal crack density was defined as the ratio of the damaged area to the whole image area. Areal crack densities for various thermoforming conditions are presented in Table 2. It should be noted that areal crack densities in Table 2 do not correspond to a unique deformation level because the last admissible thermoforming cycle at some thermoforming conditions is not identical, as presented in Table 1. Therefore, the influence of thermoforming conditions on areal crack densities is not clear in Table 2. Instead, a comparison of stress whitening values and associated areal crack densities is presented in Fig. 13. Stress whitening values were taken from Fig. 12 for the last available thermoforming cycle (e.g., third cycle stress whitening index for 0.9 mm/s forming rate and 30°C forming temperature, first cycle stress whitening index for 0.009 mm/s forming rate and 75°C forming temperature), whereas corresponding areal crack densities are given in Table 2.

Figure 13 illustrates the strong correlation between the stress whitening index and areal crack density, which is a measure of intensity of surface microdeformation features. Higher areal crack densities yield higher stress whitening levels. A master curve was also constructed, considering that when crack density is equal to zero (undamaged state), there is no stress whitening in the material ($\Delta G=0$). The master curve in Fig. 13 shows that the increase in stress whitening with respect to crack density is much larger at low crack density than that at high crack density. This is attributed to dependence of stress whitening on size of light scattering entities formed on the surface. Smaller size defects reflect more light and yield more pronounced stress whitening compare with larger ones which absorb light rather than scatter. At small crack densities (less than 10%–15%), surface defects start to form and causes larger change in appearance or stress whitening index as depicted with dashed line in Fig. 13. At large crack densities, since nearly no additional defects are formed and size of existing defects starts to increase which also hinders stress whitening, a relatively smaller change in stress whitening index with respect to crack density is observed as depicted with solid line in Fig. 13. In addition, image histograms presented in Fig. 8(*a*) also shows a larger increase in stress whitening in the first three cycles compared last two cycles which clearly indicates that at early stages (at low levels of deformation) smaller crack density yields larger change in stress whitening. According to these observations, it is clear that measured stress whitening can be correlated with the source of stress whitening, regardless of the thermoforming condition and deformation level. In development of Fig. 13, the size of individual light scattering entities was not taken into account, and the total area of damaged zones was taken as the basis for measuring the density of light scattering entities. Therefore, Fig. 13 does not describe the variation in stress whitening with size of cracks, but defines a correlation between stress whitening and overall intensity of surface deformation features.

4 Conclusions

For stress whitening quantification, a new index is defined in terms of image histograms in the logarithmic scale of gray level. The developed method produces unique numeric values for different stress whitening levels, which can be used for quantitative comparison of stress whitening under different loading conditions, and for development of relations between stress whitening level and driving forces in this phenomenon. Stress whitening in thermoformed acrylic composites was studied through a new experimental procedure developed for conventional in situ heavy-gage

Table 2 Areal crack density at various thermoforming conditions (na: not applicable)

Areal crack density (%)		Forming temperature (°C) 30	50	75	90	100	125	140
Forming rate (mm/s)	0.9	11.4	19.3	12.2	20.9	19.1	28.1	19.2
	0.09	na	na	13.1	18.0	36.7	28.4	29.2
	0.009	na	na	21.6	28.0	34.6	25.8	27.5

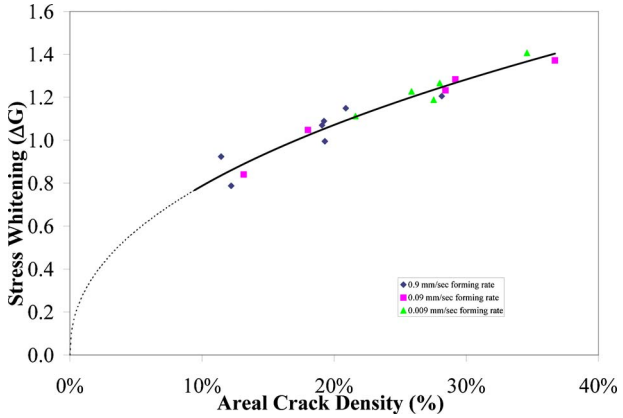

Fig. 13 Stress whitening (ΔG) versus areal crack density for various thermoforming conditions

thermoforming process. Successive thermoforming cycles on the same sample resulted in damage, which was observed as appearance and densification of light scattering entities in optical micrographs. Increase in density of these entities with increasing deformation level at each thermoforming cycle causes higher gray levels in image histograms. Microstress fields around ATH agglomerates and polymer chain mobility strongly depends on the forming temperature and forming rate. The transition in the polymer matrix deformation behavior around the glass transition temperature of PMMA and thermal microstress fields around ATH agglomerates due to the coefficient of thermal expansion are significant factors in stress whitening evolution. Stress whitening levels and microdeformation characteristics displays strong correlations. The density and size of deformation features yields different levels of stress whitening in thermoformed PMMA/ATH samples. Higher density of particle cracks at low forming temperatures results in higher stress whitening levels. Increased surface irregularity and large size voids at high forming temperatures produce lower stress whitening.

Acknowledgment

This project has been sponsored by DuPont Surface Corporation. Help received from Dr. Clyde Hutchins and Dr. Keith W. Pollak is appreciated.

Nomenclature

g_i = gray level of pixel (0–255)
n_i = number of pixels corresponding to g_ith gray level
N = total number of pixels in optical image
$\hat{\sigma}$ = standard deviation of image histogram
$\hat{\mu}$ = mean of image histogram
$\hat{\sigma}_{\text{vir}}$ = standard deviation of virgin sample's image histogram
$\hat{\mu}_{\text{vir}}$ = mean of virgin sample's image histogram
$G^{k\text{th cycle}}$ = stress whitening index of sample at kth thermoforming cycle
G^{virgin} = stress whitening index of virgin sample
ΔG = stress whitening level

References

[1] Throne, J. L., 1996, *Technology of Thermoforming*, Hanser Publishers, New York.
[2] Rosato, D. V., 2002, *Plastics Institute of America Plastics Engineering, Manufacturing and Data Handbook*, Kluwer, Dordrecht.
[3] Nathani, H., Dasari, A., and Misra, R. D. K., 2004, "On the Reduced Susceptibility to Stress Whitening Behavior of Melt Intercalated Polybutene-Clay Nanocomposites During Tensile Straining," Acta Mater., **52**, pp. 3217–3227.
[4] Pae, K. D., Chu, H. C., Lee, J. K., and Kim, J. H., 2000, "Healing of Stress-Whitening in Polyethylene and Polypropylene at or Below Room Temperature," Polym. Eng. Sci., **40**, pp. 1783–1795.
[5] Tanniru, M., and Misra, R. D. K., 2006, "Reduced Susceptibility to Stress Whitening During Tensile Deformation of Calcium Carbonate-Reinforced High Density Polyethylene Composites," Mater. Sci. Eng., A, **424**, pp. 53–70.
[6] Chandavasu, C., Xanthos, M., Sirkar, K. K., and Gogos, C. G., 2000, "Preparation of Microporous Films From Immiscible Blends via Melt Processing," J. Plast. Film Sheeting, **16**(4), pp. 288–300.
[7] Dasari, A., and Misra, R. D. K., 2004, "The Role of Micrometric Wollastonite Particles on Stress Whitening Behavior of Polypropylene Composites," Acta Mater., **52**, pp. 1683–1697.
[8] Liu, Y., Kennard, C. H. L., Truss, R. W., and Calos, N. J., 1997, "Characterization of Stress-Whitening of Tensile Yielded Isotactic Polypropylene," Polymer, **38**, pp. 2797–2805.
[9] Thridandapani, R. R., Mudaliar, A., Yuan, Q., and Misra, R. D. K., 2006, "Near Surface Deformation Associated With the Scratch in Polypropylene-Clay Nanocomposite: A Microscopic Study," Mater. Sci. Eng., A, **418**, pp. 292–302.
[10] Dasari, A., and Misra, R. D. K., 2004, "Microscopic Aspects of Surface Deformation and Fracture of High Density Polyethylene," Mater. Sci. Eng., A, **367**, pp. 248–260.
[11] Mudaliar, A., Yuan, Q., and Misra, R. D. K., 2006, "On Surface Deformation of Melt-Intercalated Polyethylene-Clay Nanocomposites During Scratching," Polym. Eng. Sci., **46**, pp. 1625–1634.
[12] Misra, R. D. K., Nathani, H., Dasari, A., Wanjale, S. D., and Jog, J. P., 2004, "The Determining Role of Clay Particles on Mechanically Induced Surface Damage and Associated Stress Whitening in Polybutene-Clay Nanocomposites," Mater. Sci. Eng., A, **386**, pp. 175–185.
[13] Hadal, R., Yuan, Q., Jog, J. P., and Misra, R. D. K., 2006, "On Stress Whitening During Surface Deformation in Clay-Containing Polymer Nanocomposites: A Microstructural Approach," Mater. Sci. Eng., A, **418**, pp. 268–281.
[14] Tillier, D. L., Meuldijk, J., Höhne, G. W. H., Frederik, P. M., Regev, O., and Koning, C. E., 2005, "About Morphology in Ethylene-Propylene(-Diene) Copolymers-Based Latexes," Polymer, **46**, pp. 7094–7108.
[15] Lalande, L., Plummer, C. J. G., Manson, J.-A. E., and Gérard, P., 2006, "Microdeformation Mechanisms in Rubber Toughened PMMA and PMMA-Based Copolymers," Eng. Fract. Mech., **73**, pp. 2413–2426.
[16] Mina, M. F., Chowdhury, M. N. K., Alam, A. K. M. M., and Michler, G. H., 2006, "Studies of Micromechanical Deformation Processes in Particle-Filled Glassy Polymer," Polym.-Plast. Technol. Eng., **45**, pp. 217–222.
[17] Cho, K., Yang, J., and Park, C. E., 1998, "The Effect of Rubber Particle Size on Toughening Behaviour of Rubber-Modified Poly(Methyl Methacrylate) With Different Test Methods," Polymer, **39**, pp. 3073–3081.
[18] Lalande, L., Plummer, C. J. G., Månson, J.-A. E., and Gérard, P., 2006, "The Influence of Matrix Modification on Fracture Mechanisms in Rubber Toughened Polymethylmethacrylate," Polymer, **47**, pp. 2389–2401.
[19] Plummer, C. J. G., Béguelin, P., and Kausch, H. H., 1999, "Microdeformation in Core-Shell Particle Modified Polymethylmethacrylates," Colloids Surf., A, **153**(1–3), pp. 551–566.
[20] Misra, R. D. K., Hadal, R., and Duncan, S. J., 2004, "Surface Damage Behavior During Scratch Deformation of Mineral Reinforced Polymer Composites," Acta Mater., **52**, pp. 4363–4376.
[21] Tanniru, M., Misra, R. D. K., Berbrand, K., and Murphy, D., 2005, "The Determining Role of Calcium Carbonate on Surface Deformation During Scratching of Calcium Carbonate-Reinforced Polyethylene Composites," Mater. Sci. Eng., A, **404**, pp. 208–220.

[22] Dasari, A., Rohrmann, J., and Misra, R. D. K., 2003, "Surface Microstructural Modification and Fracture Behavior of Tensile Deformed Polypropylene With Different Percentage Crystallinity," Mater. Sci. Eng., A, **360**, pp. 237–248.
[23] Dasari, A., Rohrmann, J., and Misra, R. D. K., 2003, "Microstructural Aspects of Surface Deformation Processes and Fracture of Tensile Strained High Isotactic Polypropylene," Mater. Sci. Eng., A, **358**, pp. 372–383.
[24] Dasari, A., Rohrmann, J., and Misra, R. D. K., 2003, "Microstructural Evolution During Tensile Deformation of Polypropylenes," Mater. Sci. Eng., A, **351**, pp. 200–213.
[25] Dasari, A., and Misra, R. D. K., 2003, "On the Strain Rate Sensitivity of High Density Polyethylene and Polypropylenes," Mater. Sci. Eng., A, **358**, pp. 356–371.
[26] Bucknall, C. B., 2001, "Applications of Microscopy to the Deformation and Fracture of Rubber-Toughened Polymers," J. Microsc., **201**, pp. 221–229.
[27] Petrich, R. P., 1973, "Impact Reinforcement of Poly(Vinyl Chloride)," Polym. Eng. Sci., **13**, pp. 248–254.
[28] Ma, X., Sauer, J. A., and Hara, M., 1995, "Poly(Methyl Methacrylate) Based Ionomers. 1. Dynamic Mechanical Properties and Morphology," Macromolecules, **28**(11), pp. 3953–3962.
[29] Ma, X., Sauer, J. A., and Hara, M., 1995, "Poly(Methyl Methacrylate) Ionomers. 2. Deformation Modes under Simple Tension," Macromolecules, **28**(16), pp. 5526–5534.
[30] Yuan, Q., Ramisetti, N., and Misra, R. D. K., 2008, "Nanoscale Near-Surface Deformation in Polymer Nanocomposites," Acta Mater., **56**(9), pp. 2089–2100.
[31] Dasari, A., Misra, R. D. K., and Rohrman, J., 2004, "Scratch Deformation Characteristics of Micrometric Wollastonite-Reinforced Ethylene-Propylene Copolymer Composites," Polym. Eng. Sci., **44**, pp. 1738–1748.
[32] Xiang, C., Sue, H. J., Chu, J., and Masuda, K., 2001, "Roles of Additives in Scratch Resistance of High Crystallinity Polypropylene Copolymers," Polym. Eng. Sci., **41**, pp. 23–31.
[33] Bensason, S., Hiltner, A., and Baer, E., 1997, "Damage Zone in PVC and PVC/MBS Blends. I. The Effect of Rubber Content and Temperature," J. Appl. Polym. Sci., **63**, pp. 703–713.
[34] Gao, G., Zhang, J., Yang, H., Zhou, C., and Zhang, H., 2006, "Deformation Mechanism of Polystyrene Toughened With Sub-Micrometer Monodisperse Rubber Particles," Polym. Int., **55**, pp. 1215–1221.
[35] Gensler, R., Plummer, C. J. G., Grein, C., and Kausch, H. H., 2000, "Influence of the Loading Rate on the Fracture Resistance of Isotactic Polypropylene and Impact Modified Isotactic Polypropylene," Polymer, **41**, pp. 3809–3819.
[36] Dasari, A., Yu, Z.-Z., Yang, M., Zhang, Q.-X., Xie, X.-L., and Mai, Y.-W., 2006, "Micro- and Nano-Scale Deformation Behavior of Nylon 66-Based Binary and Ternary Nanocomposites," Compos. Sci. Technol., **66**, pp. 3097–3114.
[37] Liu, J., Sue, H.-J., Thompson, Z. J., Bates, F. S., Dettloff, M., Jacob, G., Verghese, N., and Pham, H., 2009, "Strain Rate Effect on Toughening of Nano-Sized Pep-Peo Block Copolymer Modified Epoxy," Acta Mater., **57**(9), pp. 2691–2701.
[38] Liu, Z., Zhu, X., Wu, L., Li, Y., Qi, Z., Choy, C., and Wang, F., 2001, "Effects of Interfacial Adhesion on the Rubber Toughening of Poly(Vinyl Chloride) Part 1. Impact Tests," Polymer, **42**, pp. 737–746.
[39] Li, Z.-M., Qian, Z.-Q., Yang, M.-B., Yang, W., Xie, B.-H., and Huang, R., 2005, "Anisotropic Microstructure-Impact Fracture Behavior Relationship of Polycarbonate/Polyethylene Blends Injection-Molded at Different Temperatures," Polymer, **46**, pp. 10466–10477.
[40] Lazzeri, A., Zebarjad, S. M., Pracella, M., Cavalier, K., and Rosa, R., 2005, "Filler Toughening of Plastics. Part 1–the Effect of Surface Interactions on Physico-Mechanical Properties and Rheological Behaviour of Ultrafine $CaCo_3$/HDPE Nanocomposites," Polymer, **46**, pp. 827–844.
[41] Kody, R. S., and Martin, D. C., 1996, "Quantitative Characterization of Surface Deformation in Polymer Composites Using Digital Image Analysis," Polym. Eng. Sci., **36**, pp. 298–304.
[42] Wong, M., Moyse, A., Lee, F., and Sue, H. J., 2004, "Study of Surface Damage of Polypropylene Under Progressive Loading," J. Mater. Sci., **39**, pp. 3293–3308.
[43] Hornsby, P., and Premphet, K., 1997, "Fracture Toughness of Multiphase Polypropylene Composites Containing Rubbery and Particulate Inclusions," J. Mater. Sci., **32**, pp. 4767–4775.
[44] Lee, C.-B., and Chang, F.-C., 1992, "Toughening Behavior of Elastomer-Modified Polycarbonates Based on the J-Integral," Polym. Eng. Sci., **32**, pp. 792–803.
[45] Li, Q.-G., Xie, B.-H., Yang, W., Li, Z.-M., Zhang, W.-Q., and Yang, M.-B., 2007, "Effect of Annealing on Fracture Behavior of Poly(Propylene-Block-Ethylene) Using Essential Work of Fracture Analysis," J. Appl. Polym. Sci., **103**, pp. 3438–3446.
[46] Ferrer-Balas, D., Maspoch, M. L., Martinez, A. B., Ching, E., Li, R. K. Y., and Mai, Y. W., 2001, "Fracture Behaviour of Polypropylene Films at Different Temperatures: Assessment of the EWF Parameters," Polymer, **42**, pp. 2665–2674.
[47] Ferrer-Balas, D., Maspoch, M. L., and Mai, Y.-W., 2002, "Fracture Behaviour of Polypropylene Films at Different Temperatures: Fractography and Deformation Mechanisms Studied by SEM," Polymer, **43**, pp. 3083–3091.
[48] Gong, G., Xie, B.-H., Yang, W., Li, Z.-M., Lai, S.-M., and Yang, M.-B., 2006, "Plastic Deformation Behavior of Polypropylene/Calcium Carbonate Composites With and Without Maleic Anhydride Grafted Polypropylene Incorporated Using the Essential Work of Fracture Method," Polym. Test., **25**, pp. 98–106.
[49] Lee, J. K., Kim, J. H., Kook, H. C. C., and Pae, D., 2002, "Macroscopic Observation of Healing Process in Stress-Whitened Polypropylene Under Hydrostatic Pressure," Polym. Eng. Sci., **42**, pp. 2351–2360.
[50] Yamaguchi, M., and Nitta, K.-H., 1999, "Optical and Acoustical Investigation for Plastic Deformation of Isotactic Polypropylene/Ethylene-1-Hexene Copolymer Blends," Polym. Eng. Sci., **39**, pp. 833–840.
[51] Kasajima, M., Ito, K., and Tsutsui, M., 1981, "Influence of Temperature on Stress-Crazing of a Microcomposite Thermoplastic (Hips)," J. Macromol. Sci., Phys., **19**, pp. 649–664.
[52] Kasajima, M., Ito, K., and Tsutsui, M., 1981, "Relaxation Behavior of Stress-Crazing of a Microcomposite Thermoplastic (Hips)," J. Macromol. Sci., Phys., **19**, pp. 665–678.
[53] Squire, M., 1997, "Development of an Improved Stress Whitening Test Method for the Comparison of Polypropylene Impact Copolymers," Proceedings of the ANTEC 1997 Plastics, Plastics Saving Planet Earth, Vol. 3, pp. 2771–2774.
[54] Lee, C. D., 2005, "Structure-Property Relations in Visbroken (Peroxide Treated) Impact Polypropylene Copolymers," Proceedings of the ANTEC 2005 Plastics, Materials, Vol. 2, pp. 2035–2045.
[55] 1974, "Use of Aluminum Trihydrate in a Poly Methyl Methacrylate Article," U.S. Patent No. 3,847,865.
[56] Basaran, C., Nie, S., Hutchins, C. S., and Ergun, H., 2008, "Influence of Interfacial Bond Strength on Fatigue Life and Thermo-Mechanical Behavior of a Particulate Composite: An Experimental Study," Int. J. Damage Mech., **17**(2), pp. 123–147.
[57] Nie, S., 2005, "A Micromechanical Study of the Damage Mechanics of Acrylic Particulate Composites Under Thermomechanical Loading," Ph.D. thesis, State University of New York at Buffalo, Buffalo.
[58] Morye, S. S., 2005, "Comparison of the Thermoformability of a PPE/PP Blend With Thermoformable ABS. Part II: Large Deformation Methods," Polym. Eng. Sci., **45**, pp. 1377–1384.
[59] Stephenson, M. J., and Ryan, M. E., 1997, "Experimental Study of the Thermoforming of a Blend of Styrene-Butadiene Copolymer With Polystyrene," Polym. Eng. Sci., **37**(2), pp. 450–459.
[60] Dooling, P. J., Buckley, C. P., Rostami, S., and Zahlan, N., 2002, "Hot-Drawing of Poly(Methyl Methacrylate) and Simulation Using a Glass-Rubber Constitutive Model," Polymer, **43**, pp. 2451–2465.
[61] Münstedt, H., Kurzbeck, S., and Stange, J., 2006, "Importance of Elongational Properties of Polymer Melts for Film Blowing and Thermoforming," Polym. Eng. Sci., **46**, pp. 1190–1195.
[62] 2008, "Standard Test for Tensile Properties of Plastics," American Society for Testing and Materials, Vol. 08.01, Paper No. ASTMD638-08.
[63] Gunel, E. M., and Basaran, C., 2009, "Micro-Deformation Mechanisms in Thermoformed Alumina Trihydrate Reinforced Poly(Methyl Methacrylate)," Mater. Sci. Eng., A, **523**, pp. 160–172.
[64] Wang, Y., and Adalı, T., 2002, "Signal Processing for Magnetic Resonance Imaging and Spectroscopy, *Stochastic Model Based Image Analysis*, Marcel Dekker, New York.
[65] Adali, T., and Wang, Y., 2001, "Multimedia Image and Video Processing," *Image Analysis and Graphics for Multimedia Presentation*, CRC, Boca Raton, FL.
[66] Adali, T., Wang, Y., and Li, H., 2002, "Applications of Neural Networks to Biomedical Image Processing," *Handbook of Neural Network Signal Processing*, CRC, Boca Raton, FL.
[67] Stephens, M. A., 1974, "EDF Statistics for Goodness of Fit and Some Comparisons," J. Am. Stat. Assoc., **69**(347), pp. 730–737.
[68] Goh, T. N., Xie, M., and Tang, X. Y., 2006, "Six Sigma: Advanced Tools for Black Belts and Master Black Belts," *Data Transformation for Geometrically Distributed Quality Characteristics*, Wiley, New York.